

Electronic structure and effective mass of pristine and Cl-doped $CsPbBr_3$

Zhiyuan Wei(魏志远), Yu-Hao Wei(魏愉昊), Shendong Xu(徐申东), Shuting Peng(彭舒婷), Makoto Hashimoto, Donghui Lu(路东辉), Xu Pan(潘旭), Min-Quan Kuang(匡泯泉), Zhengguo Xiao(肖正国), and Junfeng He(何俊峰)

Citation: Chin. Phys. B, 2024, 33 (**5**): 057403. DOI: 10.1088/1674-1056/ad3c31
Journal homepage: http://cpb.iphy.ac.cn; http://iopscience.iop.org/cpb

What follows is a list of articles you may be interested in

Superconductivity in kagome metal $ThRu_3Si_2$

Yi Liu(刘艺), Jing Li(厉静), Wu-Zhang Yang(杨武璋), Jia-Yi Lu(卢佳依), Bo-Ya Cao(曹博雅), Hua-Xun Li(李华旬), Wan-Li Chai(柴万力), Si-Qi Wu(武思祺), Bai-Zhuo Li(李佰卓), Yun-Lei Sun(孙云蕾), Wen-He Jiao(焦文鹤), Cao Wang(王操), Xiao-Feng Xu(许晓峰), Zhi Ren(任之), and Guang-Han Cao(曹光旱)

Chin. Phys. B, 2024, 33 (**5**): 057401. DOI: 10.1088/1674-1056/ad1c5e

Distinct behavior of electronic structure under uniaxial strain in $BaFe_2As_2$

Jiajun Li(李佳俊), Giao Ngoc Phan, Xingyu Wang(王兴玉), Fazhi Yang(杨发枝), Quanxin Hu(胡全欣), Ke Jia(贾可), Jin Zhao(赵金), Wenyao Liu(刘文尧), Renjie Zhang(张任杰), Youguo Shi(石友国), Shiliang Li(李世亮), Tian Qian(钱天), and Hong Ding(丁洪)

Chin. Phys. B, 2024, 33 (**1**): 017401. DOI: 10.1088/1674-1056/acd8af

Experimental observation of pseudogap in a modulation-doped Mott insulator: Sn/Si(111)-($\sqrt{30}\times\sqrt{30}$)*R*30°

Yan-Ling Xiong(熊艳翎), Jia-Qi Guan(关佳其), Rui-Feng Wang(汪瑞峰), Can-Li Song(宋灿立), Xu-Cun Ma(马旭村), and Qi-Kun Xue(薛其坤)

Chin. Phys. B, 2022, 31 (**6**): 067401. DOI: 10.1088/1674-1056/ac65f2

Measurement of electronic structure in van der Waals ferromagnet $Fe_{5-x}GeTe_2$

Kui Huang(黄逵), Zhenxian Li(李政贤), Deping Guo(郭的坪), Haifeng Yang(杨海峰), Yiwei Li(李一苇),Aiji Liang(梁爱基), Fan Wu(吴凡), Lixuan Xu(徐丽璇), Lexian Yang(杨乐仙), Wei Ji(季威),Yanfeng Guo(郭艳峰), Yulin Chen(陈宇林), and Zhongkai Liu(柳仲楷)

Chin. Phys. B, 2022, 31 (**5**): 057404. DOI: 10.1088/1674-1056/ac5c3c

Surface-induced orbital-selective band reconstruction in kagome superconductor CsV_3Sb_5

Linwei Huai(淮琳崴), Yang Luo(罗洋), Samuel M. L. Teicher, Brenden R. Ortiz, Kaize Wang(王铠泽),Shuting Peng(彭舒婷), Zhiyuan Wei(魏志远), Jianchang Shen(沈建昌), Bingqian Wang(王冰倩), Yu Miao(缪宇),Xiupeng Sun(孙秀鹏), Zhipeng Ou(欧志鹏), Stephen D. Wilson, and Junfeng He(何俊峰)

Chin. Phys. B, 2022, 31 (**5**): 057403. DOI: 10.1088/1674-1056/ac4f50

RAPID COMMUNICATION

Electronic structure and effective mass of pristine and Cl-doped $CsPbBr_3$

Zhiyuan Wei(魏志远)[1,†], Yu-Hao Wei(魏愉昊)[2,†], Shendong Xu(徐申东)[3,†], Shuting Peng(彭舒婷)[1], Makoto Hashimoto[4], Donghui Lu(路东辉)[4], Xu Pan(潘旭)[3], Min-Quan Kuang(匡泯泉)[2,‡], Zhengguo Xiao(肖正国)[1,§], and Junfeng He(何俊峰)[1,¶]

[1] *Department of Physics and CAS Key Laboratory of Strongly-coupled Quantum Matter Physics, University of Science and Technology of China, Hefei* 230026, *China*

[2] *Chongqing Key Laboratory of Micro & Nano Structure Optoelectronics, and School of Physical Science and Technology, Southwest University, Chongqing* 400715, *China*

[3] *Key Laboratory of Photovoltaic and Energy Conservation Materials, Institute of Applied Technology, Hefei Institutes of Physical Science, Chinese Academy of Sciences, Hefei* 230031, *China*

[4] *Stanford Synchrotron Radiation Lightsource and Stanford Institute for Materials and Energy Sciences, SLAC National Accelerator Laboratory, Menlo Park, California* 94025, *USA*

(Received 11 January 2024; revised manuscript received 7 March 2024; accepted manuscript online 10 April 2024)

Organic–inorganic lead halide perovskites (LHPs) have attracted great interest owing to their outstanding optoelectronic properties. Typically, the underlying electronic structure would determinate the physical properties of materials. But as for now, limited studies have been done to reveal the underlying electronic structure of this material system, comparing to the huge amount of investigations on the material synthesis. The effective mass of the valance band is one of the most important physical parameters which plays a dominant role in charge transport and photovoltaic phenomena. In pristine $CsPbBr_3$, the Fröhlich polarons associated with the Pb–Br stretching modes are proposed to be responsible for the effective mass renormalization. In this regard, it would be very interesting to explore the electronic structure in doped LHPs. Here, we report high-resolution angle-resolved photoemission spectroscopy (ARPES) studies on both pristine and Cl-doped $CsPbBr_3$. The experimental band dispersions are extracted from ARPES spectra along both $\bar{\Gamma}$–$\bar{M}$–$\bar{\Gamma}$ and $\bar{X}$–$\bar{M}$–$\bar{X}$ high symmetry directions. DFT calculations are performed and directly compared with the ARPES data. Our results have revealed the band structure of Cl-doped $CsPbBr_3$ for the first time, which have also unveiled the effective mass renormalization in the Cl-doped $CsPbBr_3$ compound. Doping dependent measurements indicate that the chlorine doping could moderately tune the renormalization strength. These results will help understand the physical properties of LHPs as a function of doping.

Keywords: lead halide perovskites, electronic structure, effective mass

PACS: 74.25.Jb, 79.60.–i, 71.20.–b, 74.20.Pq **DOI:** 10.1088/1674-1056/ad3c31

1. Introduction

Lead halide perovskites are a class of materials with the formula ABX_3, in which A is a cation, B is lead and X represents halogen.[1] Recently, lead halide perovskites (LHPs) have attracted intensive interest due to their potential applications in solar cells,[2–5] light-emitting diodes,[6–8] photon detection and laser devices.[9–12] In particular, solar cells with an LHP as the photovoltaic active materials have been certificated to achieve efficiency approaching 25% only several years after the initially reported efficiency of 4%.[13–18] In comparison, GaAs keeps a photoconversion efficiency record of $\sim$ 29% after almost 6 decades of study from the initial efficiency of 4%.[19,20] Another large advantage of LHPs is the low cost compared with other high efficiency materials, because the LHPs are easy to synthesize by simple solution methods.[21]

Although the photoconversion efficiency of LHPs solar cell has been improved a lot, but a full understanding of the underlying microscopic mechanism is still lacking. In order to further enhance the quantum efficiency of LHPs, the underlying physical parameters should be carefully investigated. The effective mass of the carriers is an essential parameter in semiconductors, which plays a dominant role in both charge transport and optical absorption. In the past a few years, several studies have been carried out to investigate the electronic structure of LHPs by angle-resolved photoemission spectroscopy (ARPES),[22–27] which is one of the most direct ways to detect the band structure and effective mass.[28,29] In $CsPbBr_3$, ARPES results reveal that the effective mass is $\sim$ 50% heavier than that calculated by the DFT. This effect has been explained by the formation of Fröhlich polarons.[27,30,31] The *ab initio* electron–phonon coupling calculations show that the Fröhlich polarons are dominated by

[†]These authors contributed equally to this work.
[‡]Corresponding author. E-mail: mqkuang@swu.edu.cn
[§]Corresponding author. E-mail: zhengguo@ustc.edu.cn
[¶]Corresponding author. E-mail: jfhe@ustc.edu.cn

© 2024 Chinese Physical Society and IOP Publishing Ltd

Pb–Br stretching modes, which would induce the effective mass renormalization.[27] However, the doping dependence of the effective mass renormalization is still lacking.[32] In this article, we report a systematic study on the valance band effective mass for $CsPbBr_3$ and $CsPbClBr_2$ along both $\bar{\Gamma}$–$\bar{M}$–$\bar{\Gamma}$ and $\bar{X}$–$\bar{M}$–$\bar{X}$ directions. These results reveal the role of element doping on the influence of carries effective mass in LHPs, which can also provide insights into the understanding of the enhanced quantum efficiency.

2. Experimental detail and results

Single crystals of $CsPbBr_3$ and $CsPbClBr_2$ were prepared as follows.[11,33,34] (i) Firstly, CsBr and $PbBr_2$ were dissolved in a 1:2 molar ratio in dimethyl sulfoxide (DMSO) solvent to obtain a solution with a lead ion concentration of 1 mol/L. Stir thoroughly at room temperature until fully dissolved. Then, any undissolved material was removed from the solution using a 0.2-micron organic syringe filter to obtain a clear solution. (ii) Next, 1 mL of a mixed solution of dimethylformamide (DMF) and cyclohexanol (CyOH) was added to the clear solution (DMF:CyOH = 1.8:1, by volume) and stirred until fully dissolved. (iii) An appropriate amount of the prepared precursor solution was put in a 5 mL glass vial, the vial was sealed tightly and wrapped with sealing tape, then placed in an oil bath. The oil bath was gradually heated to around 70 °C and this temperature was kept for 48 h. Visible crystals should form during this time. (iv) When the growth was complete, the crystals were removed and the crystal surfaces were rinsed with ether, then placed in a vacuum drying oven for drying. The preparation process of $CsPbClBr_2$ was the same as above except that the CsBr was replaced by CsCl and half amount of the mixed solution (with the same ratio) was used. ARPES measurements were carried out at Beamline 5-2 of the Stanford Synchrotron Radiation Lightsource (SSRL) of SLAC National Accelerator Laboratory with a photon energy of 33.5 eV. The total energy resolution was ~ 18 meV and the base pressure was better than 3×10^{-11} torr. All samples were cleaved *in situ* with fresh cleaving surfaces and measured at room temperature (~ 300 K) to avoid the possible charging effect. The Fermi level was determined by measuring the polycrystalline Au in electrical contact with the samples. First-principles calculations for $CsPbBr_3$ and $CsPbClBr_2$ were carried out by using the Vienna *ab initio* simulation package (VASP) in the framework of density functional theory (DFT).[35,36] The generalized gradient approximation (GGA) of the Perdew–Burke–Ernzerhof functional was adopted as the exchange–correlation functional.[37–39] The plane wave truncation energy was selected as 400 eV and the convergence accuracy of the self-consistent iteration was set as 1×10^{-6} eV/atom. The force convergence criterion was -0.01 eV/Å and the BZ was sampled with $11 \times 11 \times 11$ k-mesh for structural relaxation and self-consistent calculation of $CsPbBr_3$ and $CsPbClBr_2$. The Br/Cl substitution effects were treated within the virtual crystal approximation (VCA),[40] and the optimized lattice constants for $CsPbBr_3$ and $CsPbClBr_2$ were $a = b = c = 5.997$ Å and 5.932 Å, respectively. The Green's function iterative method implemented in the WANNIERTOOLS (WT) software package[41] was adopted to demonstrate the surface electronic properties.

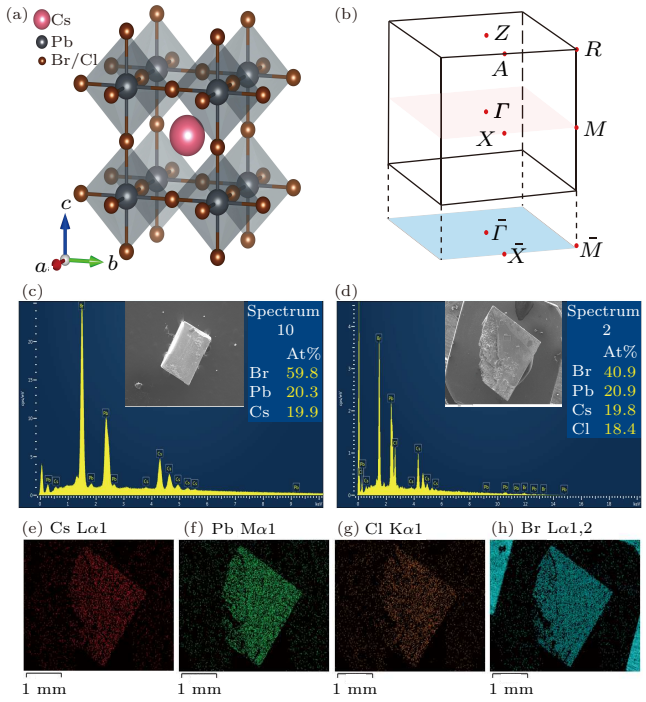


Fig. 1. Characterizations of the $CsPbCl_xBr_{3-x}$ single crystals. (a) Schematic of the cubic crystal structure of $CsPbCl_xBr_{3-x}$. The $[PbBr_6]^{4-}$ octahedra are highlighted in gray. (b) 3D Brillouin zone of the cubic phase of $CsPbCl_xBr_{3-x}$. (c) Energy-dispersive x-ray spectroscopy (EDS) results for $CsPbBr_3$. Insert: scanning electron microscopy (SEM) image of the $CsPbBr_3$ single crystal. Panel (d) the same as panel (c) but for $CsPbClBr_2$. (e)–(h) EDS mapping of the $CsPbClBr_2$ single crystal. The distribution of Cs, Pb, Cl, and Br elements are indicated by red, green, orange and blue, respectively.

The crystal structure of $CsPbCl_xBr_{3-x}$ is shown in Fig. 1(a), different elements are represented by different colors. The three-dimensional (3D) Brillouin zone is plotted in Fig. 1(b). The Γ–M–X–Γ plane locates at $k_z = 0$ and the Z–R–A–Z plane locates at $k_z = \pi/c$. The projected 2D Brillouin zone is indicated by the $\bar{\Gamma}$–$\bar{M}$–$\bar{X}$–$\bar{\Gamma}$ plane. To examine the stoichiometry of the elements in pristine and Cl-doped sample, we have carried out energy-dispersive x-ray spectroscopy (EDS) on these samples as shown in Figs. 1(c) and 1(d) respectively. The scanning electron microscopy (SEM) topography images are shown in the inserts. It is obvious that Cl peaks are observed in the Cl-doped sample, demonstrating that the Cl atoms are indeed doped into the sample. We have calculated the stoichiometric ratio in both pristine and Cl-doped samples. In the pristine sample, the atomic ratio for Cs:Pb:Br is $\sim$ 1:1:3, which is consistent with the nomi-

nal ratio in $CsPbBr_3$. In the Cl-doped sample, the atomic ratio is Cs:Pb:Cl:Br $\sim$ 1:1:1:2, which is also consistent with the nominal ratio in $CsPbClBr_2$. We have also carried out EDS mapping on the Cl-doped $CsPbClBr_2$ sample. As shown in Figs. 1(e)–1(h), all elements are distributed uniformly in the single crystal samples.

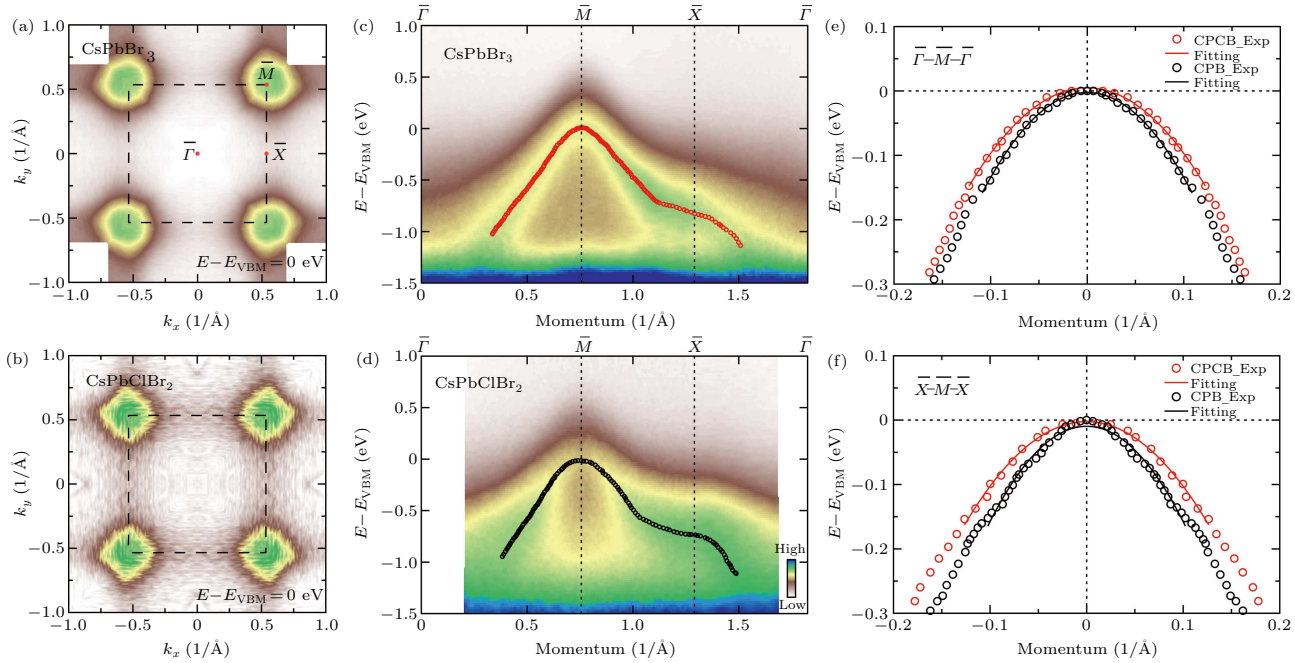


Fig. 2. ARPES spectra of $CsPbBr_3$ and $CsPbClBr_2$. (a) and (b) Symmetrized constant energy map at $E = E_{VBM}$ for $CsPbBr_3$ and $CsPbClBr_2$, respectively. (c) and (d) Electron energy band of $CsPbBr_3$ and $CsPbClBr_2$ along the $\bar{\Gamma}$–$\bar{M}$–$\bar{X}$–$\bar{\Gamma}$, respectively. The extracted band dispersions are appended to the spectra. (e) Extracted band dispersions along the $\bar{\Gamma}$–$\bar{M}$–$\bar{\Gamma}$. The data of $CsPbBr_3$ ($CsPbClBr_2$) are shown in black (red). The parabolic fitting results are shown by solid lines. Panel (f) the same as panel (e) but along the $\bar{X}$–$\bar{M}$–$\bar{X}$ direction.

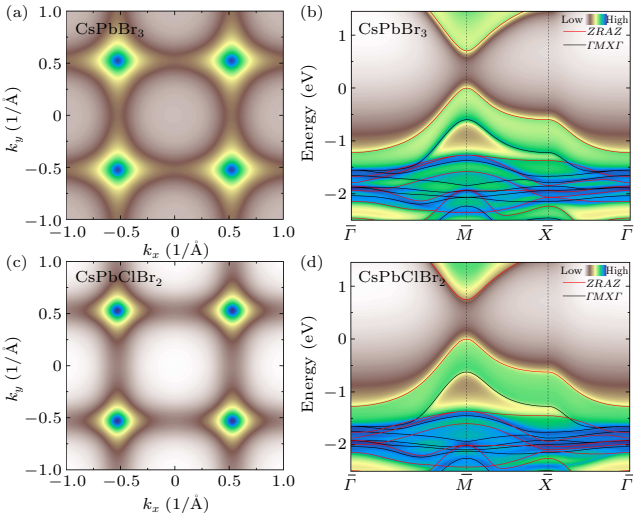


Fig. 3. DFT calculations for $CsPbBr_3$ and $CsPbClBr_2$. (a) Calculated constant energy map of $CsPbBr_3$ at $E = E_{VBM}$ with $k_z = \pi/c$. (b) Calculated energy band of $CsPbBr_3$ along the $\bar{\Gamma}$–$\bar{M}$–$\bar{X}$–$\bar{\Gamma}$. Black lines represent the DFT band dispersion along the Γ–M–X–Γ ($k_z = 0$). Red lines represent the DFT band dispersion along the Z–R–A–Z ($k_z = \pi/c$). Panels (c) and (d) are the same as panels (a) and (b) but for $CsPbClBr_2$.

Constant energy maps of $CsPbBr_3$ and $CsPbClBr_2$ at the top of the valance band (valance band maximum, VBM) are shown in Figs. 2(a) and 2(b), respectively. The dashed lines indicate the Brillouin zone of the cubic phase of $CsPbBr_3$. It is clear that the valance band maximum is always at the $\bar{M}$ point, regardless of the Cl doping. The energy bands of $CsPbBr_3$ and $CsPbClBr_2$ along $\bar{\Gamma}$–$\bar{M}$–$\bar{X}$–$\bar{\Gamma}$ are presented in Figs. 2(c) and 2(d), respectively. For simplicity, we follow the earlier study to set the energy of the valance band maximum as zero ($E - E_{VBM} = 0$).[27] The overall band structure is similar in both samples, with a hole-like band around $\bar{M}$ and a Van Hove singularity around $\bar{X}$ point. In order to quantitatively compare the band dispersion as a function of doping, we extract the dispersion near the valance band maximum and present them in Figs. 2(e) and 2(f). Shown in Fig. 2(e) is the band dispersion along the $\bar{\Gamma}$–$\bar{M}$–$\bar{\Gamma}$. Pristine and Cl-doped data are represented by black and red circles, respectively. To examine the effective mass, parabolic fittings are carried out near the valance band maximum, following the earlier study.[27] The band dispersions along $\bar{X}$–$\bar{M}$–$\bar{X}$ are shown in Fig. 2(f), where parabolic fittings are also performed. Following the earlier study, these measurements are carried out with a photon energy of 33.5 eV, which corresponds to $k_z \sim 0.5$ Å^{-1} near the R point.[27]

For comparison, we have carried out first-principles calculations. Figures 3(a) and 3(c) are constant energy maps for $CsPbBr_3$ and $CsPbClBr_2$ at the valance band maximum with the same k_z as that in the experiment. Both of them are similar to the experimental results in Figs. 2(a) and 2(b). Figures 3(b) and 3(d) are calculated energy bands for $CsPbBr_3$ and $CsPbClBr_2$ along $\bar{\Gamma}$–$\bar{M}$–$\bar{X}$–$\bar{\Gamma}$. The band dispersion along Z–R–A–Z ($k_z = \pi/c$) is shown by red lines and the band dispersion along Γ–M–X–Γ ($k_z = 0$) is indicated by black lines.

Following the experimental results, the energy of the valance band maximum is set as zero. A resemblance is clearly seen between the calculations and the experiments, which further confirms that the overall band structure remains similar with the Cl doping. These results also establish a basis for a quantitative comparison of the effective mass as a function of doping.

In order to carefully examine the renormalization of the effective mass, both the experimental (solid lines) and calculated (dashed lines) bands are shown in Figs. 4(a) and 4(b) for comparison. First, the experimental effective mass is significantly larger than the one from the DFT calculation. This point remains valid in both pristine and Cl-doped samples. Second, the experimental effective mass becomes larger with Cl doping, whereas the calculated one exhibits little change as a function of doping. As shown in Fig. 4(a), parabolic fittings[27] of the experimental results give rise to an effective mass $m^* = 0.29m_e$ for $CsPbBr_3$ along the $\bar{\Gamma}$–$\bar{M}$–$\bar{\Gamma}$ direction (see Fig. S1(a)). This effective mass is further increased to $m^* = 0.37m_e$ in $CsPbClBr_2$ (see Fig. S1(b)). On the other hand, the parabolic fittings of the DFT bands along $\bar{\Gamma}$–$\bar{M}$–$\bar{\Gamma}$ show a bare effective mass $m_0 = 0.17m_e$ for both pristine and Cl-doped samples (see Figs. S1(c) and S1(d)). The same is true for the bands along another high symmetry direction $\bar{X}$–$\bar{M}$–$\bar{X}$. As shown in Fig. 4(b), the experimental data give an effective mass $m^* = 0.26m_e$ for $CsPbBr_3$ and $m^* = 0.38m_e$ for $CsPbClBr_2$, respectively (see Figs. S2(a) and S2(b)). The DFT calculations show a bare effective mass $m_0 = 0.17m_e$ for both $CsPbBr_3$ and $CsPbClBr_2$ along the $\bar{X}$–$\bar{M}$–$\bar{X}$ direction (see Figs. S2(c) and S2(d)). In order to visualize the evolution of the effective mass, the above results are summarized in Fig. 4(c) for comparison.

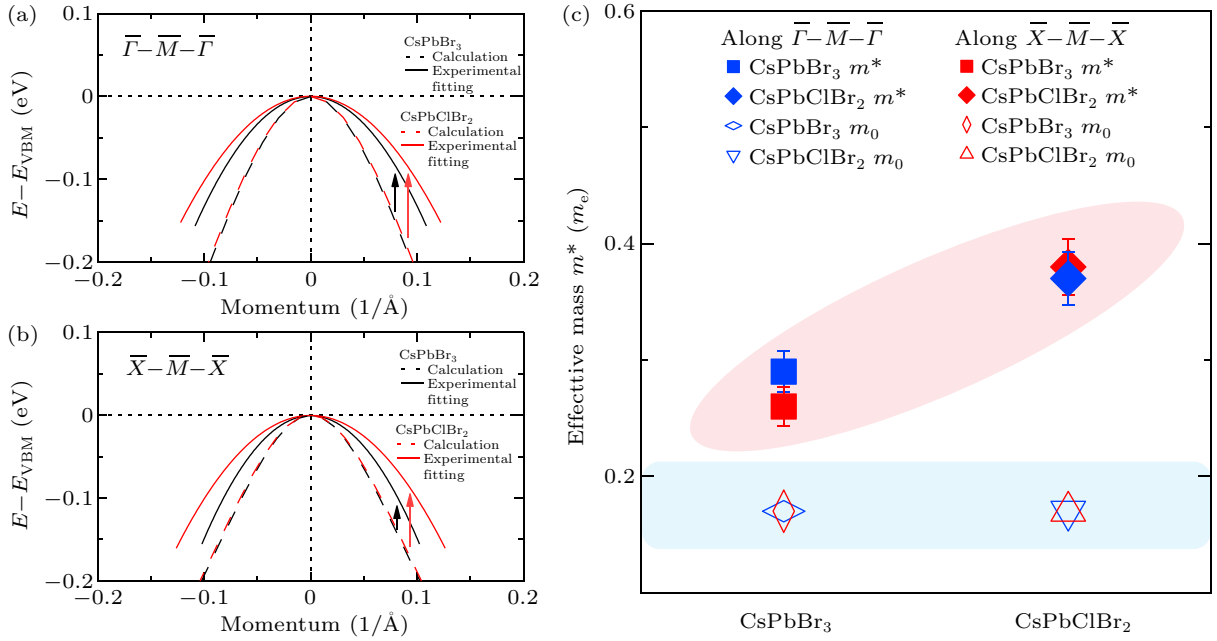


Fig. 4. Comparison of the effective mass for pristine and Cl-doped $CsPbBr_3$. (a) Comparison of DFT and experimental results for $CsPbBr_3$ and $CsPbClBr_2$ along $\bar{\Gamma}$–$\bar{M}$–$\bar{\Gamma}$. DFT results for $CsPbBr_3$ and $CsPbClBr_2$ are plotted by dashed black and red lines, respectively. The experimental results (from the parabolic fitting) for $CsPbBr_3$ and $CsPbClBr_2$ are shown by solid black and red lines, respectively. Panel (b) the same as panel (a) but along $\bar{X}$–$\bar{M}$–$\bar{X}$. (c) Summary of both experimental and theoretical effective mass for $CsPbBr_3$ and $CsPbClBr_2$. Data along $\bar{\Gamma}$–$\bar{M}$–$\bar{\Gamma}$ ($\bar{X}$–$\bar{M}$–$\bar{X}$) are shown in blue (red).

3. Discussion

Next, we discuss the implications of our results. At room temperature, $CsPbBr_3$ has an orthorhombic crystal structure, which is different from the cubic structure. A cubic to orthorhombic phase transition occurs below 360 K.[42–44] However, an earlier study reports that the electronic structure of $CsPbBr_3$ follows the periodicity of the cubic phase rather than the orthorhombic phase at room temperature.[27] Our results have confirmed this point and extended this observation to the Cl-doped sample. For comparison, the first-principles calculations have also been carried out for the cubic phase structure. With these points clarified, we focus on the renormalization of the effective mass. First, for the pristine sample, the experimental effective mass ($m^* = 0.29m_e$) is much heavier than the bare effective mass ($m^* = 0.17m_e$) along the $\bar{\Gamma}$–$\bar{M}$–$\bar{\Gamma}$ direction. This is consistent with the earlier study, where an effective mass of $0.26m_e$ was reported.[27] Our results further reveal that the effective mass along the $\bar{X}$–$\bar{M}$–$\bar{X}$ direction ($m^* = 0.26m_e$) is also significantly heavier than the bare effective mass. These results are consistent with the theoretical proposal that the enhancement of the effective mass is caused by the Fröhlich polarons.[27] Second, our experimental results reveal that the effective mass is further enhanced in the Cl-doped sample. One possibility is that the Cl element substitu-

tion changes the lattice and the band structure of the crystal. As such, the effective mass would also change with Cl doping. However, the DFT calculations indicate that the band structures of the pristine and Cl-doped samples are similar, and the associated bare effective mass shows little change with Cl doping. Another possibility is to consider the scenario of Fröhlich polarons.[27,30] On the one hand, the Pb–Br stretching modes may change with Cl element substitution, which would naturally change the polarons. On the other hand, the electron–phonon coupling strength may change with the Cl doping, which would also affect the effective mass of the electrons. In a practical point of view, our results indicate that the electron–phonon interaction and the effective mass of the electrons in $CsPbBr_3$ can be manipulated by a simple element substitution, which would help the material design and synthesis in LHPs.

4. Conclusion

By performing high resolution ARPES measurements, we have revealed the doping dependence of the electronic structure in $CsPbBr_3$ for the first time. The extracted effective mass from the experiments is significantly larger than the bare effective mass from DFT calculations. The experimental effective mass further increases with Cl doping. Our results are consistent with the scenario that the renormalization of the effective mass is due to electron–phonon interaction. They also shed light on the manipulation of the electronic structure of LHPs via chemical element doping.

Acknowledgments

Project supported by the International Partnership Program of the Chinese Academy of Sciences (Grant No. 123GJHZ2022035MI) and the Fundamental Research Funds for the Central Universities (Grant Nos. WK3510000015 and WK3510000012).

References

[1] Wells A F 1984 *Structural Inorganic Chemistry* 5th edn. (Oxford: Oxford University Press)
[2] Li B, Zhang Y, Fu L, Yu T, Zhou S, Zhang L and Yin L 2018 *Nat. Commun.* **9** 1076
[3] Noh J H, Im S H, Heo J H, Mandal T N and Seok S I 2013 *Nano Lett.* **13** 1764
[4] Tong G, Ono L K and Qi Y 2020 *Energy Technol.* **8** 1900961
[5] Wang Z, Zeng L, Zhu T, Chen H, Chen B, Kubicki D J, Balvanz A, Li C, Maxwell A and Ugur E 2023 *Nature* **618** 74
[6] Du X, Wu G, Cheng J, Dang H, Ma K, Zhang Y W, Tan P F and Chen S 2017 *RSC Adv.* **7** 10391
[7] Lin K, Xing J, Quan L N, de Arquer F P G, Gong X, Lu J, Xie L, Zhao W, Zhang D and Yan C 2018 *Nature* **562** 245
[8] Zheng W, Wan Q, Liu M, Zhang Q, Zhang C, Yan R, Feng X, Kong L and Li L 2021 *J. Phys. Chem. C* **125** 3110
[9] Yakunin S, Protesescu L, Krieg F, Bodnarchuk M I, Nedelcu G, Humer M, De Luca G, Fiebig M, Heiss W and Kovalenko M V 2015 *Nat. Commun.* **6** 8056
[10] Pan L, Pandey I R, Miceli A, Klepov V V, Chung D Y and Kanatzidis M G 2023 *Adv. Opt. Mater.* **11** 2202946
[11] Dirin D N, Cherniukh I, Yakunin S, Shynkarenko Y and Kovalenko M V 2016 *Chem. Mater.* **28** 8470
[12] Pan L, He Y, Klepov V V, Michael C and Kanatzidis M G 2022 *IEEE Trans. Med. Imaging* **41** 3053
[13] Kojima A, Teshima K, Shirai Y and Miyasaka T 2009 *J. Am. Chem. Soc.* **131** 6050
[14] Yang W S, Noh J H, Jeon N J, Kim Y C, Ryu S, Seo J and Seok S I 2015 *Science* **348** 1234
[15] Hou Y, Aydin E, De Bastiani M, Xiao C, Isikgor F H, Xue D J, Chen B, Chen H, Bahrami B and Chowdhury A H 2020 *Science* **367** 1135
[16] Köhnen E, Jošt M, Morales-Vilches A B, Tockhorn P, Al-Ashouri A, Macco B, Kegelmann L, Korte L, Rech B and Schlatmann R 2019 *Sustain. Energy Fuels* **3** 1995
[17] McMeekin D P, Sadoughi G, Rehman W, Eperon G E, Saliba M, Hörantner M T, Haghighirad A, Sakai N, Korte L and Rech B 2016 *Science* **351** 151
[18] Sahli F, Werner J, Kamino B A, Bräuninger M, Monnard R, Paviet-Salomon B, Barraud L, Ding L, Diaz Leon J J and Sacchetto D 2018 *Nat. Mater.* **17** 820
[19] Jenny D, Loferski J and Rappaport P 1956 *Phys. Rev.* **101** 1208
[20] Yablonovitch E, Miller O D and Kurtz S R 2012 38*th IEEE Photovoltaic Specialists Conference* pp. 001556–001559
[21] Brenner T M, Egger D A, Kronik L, Hodes G and Cahen D 2016 *Nat. Rev. Mater.* **1** 15007
[22] Komesu T, Huang X, Paudel T R, Losovyj Y B, Zhang X, Schwier E F, Kojima Y, Zheng M, Iwasawa H and Shimada K 2016 *J. Phys. Chem. C* **120** 21710
[23] Niesner D, Wilhelm M, Levchuk I, Osvet A, Shrestha S, Batentschuk M, Brabec C and Fauster T 2016 *Phys. Rev. Lett.* **117** 126401
[24] Sajedi M, Krivenkov M, Marchenko D, Varykhalov A, Sánchez-Barriga J, Rienks E and Rader O 2020 *Phys. Rev. B* **102** 081116
[25] Yang J P, Meissner M, Yamaguchi T, Zhang X Y, Ueba T, Cheng L W, Ideta S, Tanaka K, Zeng X H and Ueno N 2018 *Sol. RRL* **2** 1800132
[26] Zu F, Amsalem P, Egger D A, Wang R, Wolff C M, Fang H, Loi M A, Neher D, Kronik L and Duhm S 2019 *J. Phys. Chem. Lett.* **10** 601
[27] Puppin M, Polishchuk S, Colonna N, Crepaldi A, Dirin D N, Nazarenko O, De Gennaro R, Gatti G, Roth S, Barillot T, Poletto L, Xian R P, Rettig L, Wolf M, Ernstorfer R, Kovalenko M V, Marzari N, Grioni M and Chergui M 2020 *Phys. Rev. Lett.* **124** 206402
[28] Sobota J A, He Y and Shen Z X 2021 *Rev. Mod. Phys.* **93** 025006
[29] Damascelli A, Hussain Z and Shen Z X 2003 *Rev. Mod. Phys.* **75** 473
[30] Fröhlich H, Pelzer H and Zienau S 1950 *Lond. Edinb. Dublin Phil. Mag. J. Sci.* **41** 221
[31] Iaru C M, Brodu A, van Hoof N J, Ter Huurne S E, Buhot J, Montanarella F, Buhbut S, Christianen P C, Vanmaekelbergh D and de Mello Donega C 2021 *Nat. Commun.* **12** 5844
[32] Niesner D 2020 *APL Mater.* **8** 090704
[33] Yu J, Liu G, Chen C, Li Y, Xu M, Wang T, Zhao G and Zhang L 2020 *J. Mater. Chem. C* **8** 6326
[34] Wang F, Zhang H, Sun Q, Hafsia A B, Chen Z, Zhang B, Xu Y and Jie W 2020 *Cryst. Growth Des.* **20** 1638
[35] Kresse G and Hafner J 1994 *Phys. Rev. B* **49** 14251
[36] Kresse G and Furthmüller J 1996 *Phys. Rev. B* **54** 11169
[37] Perdew J P, Burke K and Ernzerhof M 1996 *Phys. Rev. Lett.* **77** 3865
[38] Perdew J P, Burke K and Ernzerhof M 1998 *Phys. Rev. Lett.* **80** 891
[39] Ernzerhof M and Scuseria G E 1999 *J. Chem. Phys.* **110** 5029
[40] Bellaiche L and Vanderbilt D 2000 *Phys. Rev. B* **61** 7877
[41] Wu Q, Zhang S, Song H F, Troyer M and Soluyanov A A 2018 *Comput. Phys. Commun.* **224** 405
[42] Stoumpos C C, Malliakas C D, Peters J A, Liu Z, Sebastian M, Im J, Chasapis T C, Wibowo A C, Chung D Y and Freeman A J 2013 *Cryst. Growth Design* **13** 2722
[43] Cottingham P and Brutchey R L 2016 *Chem. Commun.* **52** 5246
[44] He Y, Matei L, Jung H J, McCall K M, Chen M, Stoumpos C C, Liu Z, Peters J A, Chung D Y and Wessels B W 2018 *Nat. Commun.* **9** 1609